nature geoscience

ARTICLES

PUBLISHED ONLINE: 23 JANUARY 2011 | DOI: 10.1038/NGEO1064

Magmatic–hydrothermal origin of Nevada's Carlin-type gold deposits

John L. Muntean[1]*, Jean S. Cline[2], Adam C. Simon[2] and Anthony A. Longo[2]

The Eocene epoch in the Great Basin of western North America was a period of profuse magmatism and hydrothermal activity. During that period, the Carlin-type gold deposits in Nevada were produced, Earth's second largest concentration of gold after deposits in South Africa. The characteristics of the Carlin-type deposits have been documented, but a widely acceptable explanation for their genesis is outstanding. Here we integrate microanalyses of ore minerals, experimental data that describe metal partitioning, and published age and isotopic data, to suggest that the gold is sourced from magma. We relate gold deposition to a change from shallow subduction to renewed magmatism and the onset of extension. We propose that upwelling asthenosphere impinged on a strongly modified subcontinental lithospheric mantle, generating magmas that released gold-bearing fluids at depths of 10 to 12 km. The rising aqueous fluids with elevated hydrogen sulphide concentrations and a high ratio of gold to copper underwent phase changes and mixed with meteoric water. Within a few kilometres of the surface, the fluids dissolved and sulphidized carbonate wall rocks, leading to deposition of gold-bearing pyrite. We conclude that the large number and size of Carlin-type deposits in Nevada is the result of an unusual convergence of a specific geologic setting, together with a tectonic trigger that led to extremely efficient transport and deposition of gold.

The Eocene epoch in the Great Basin of western North America was a period of intense hydrothermal activity brought on by a shift from shallow subduction and compressional tectonics to renewed magmatism coincident with extensional tectonics. The most important economic manifestation of this activity is the formation of Carlin-type gold deposits (CTGDs) in northern Nevada, which contain over 6,000 tons of gold (Au), constituting the second largest concentration of Au in the world[1] (Fig. 1). The deposits account for ~6% of annual worldwide production, making the United States the fourth largest producer of Au. CTGDs are hydrothermal replacement bodies hosted primarily by lower Palaeozoic miogeoclinal carbonate rocks, in which Au occurs in solid solution or as submicrometre particles in pyrite. Salient features of the four largest clusters of deposits (Carlin trend, Cortez, Getchell, Jerritt Canyon; Fig. 1), which account for >90% of the Au in CTGDs worldwide, are listed in Table 1. These characteristics indicate that common processes led to the formation and transportation of Au-bearing hydrothermal fluids and deposition of Au; however, these ubiquitous features have not been sufficiently diagnostic to yield a widely accepted genetic model. Two endmember models that describe the proposed origin of Au in CTGDs include: (1) magmatic–hydrothermal models, in which Au was derived from magmas; and (2) amagmatic models, wherein Au was sourced from the crust by meteoric or metamorphic waters[1].

Here, we propose a model for the origin of CTGDs that (1) describes the formation of a primitive ore fluid and tracks that fluid through Au deposition, and (2) relates the fluid and CTGDs to subduction processes and deep crustal magma evolution brought about by a change in tectonics. This model evolved in response to new data we generated and recently published data that demonstrate a closer temporal and spatial link between deposit formation and magmatism than was previously reported. These data include geochronologic data, which demonstrate that formation of the CTGDs tracked the southwestern sweep of Eocene

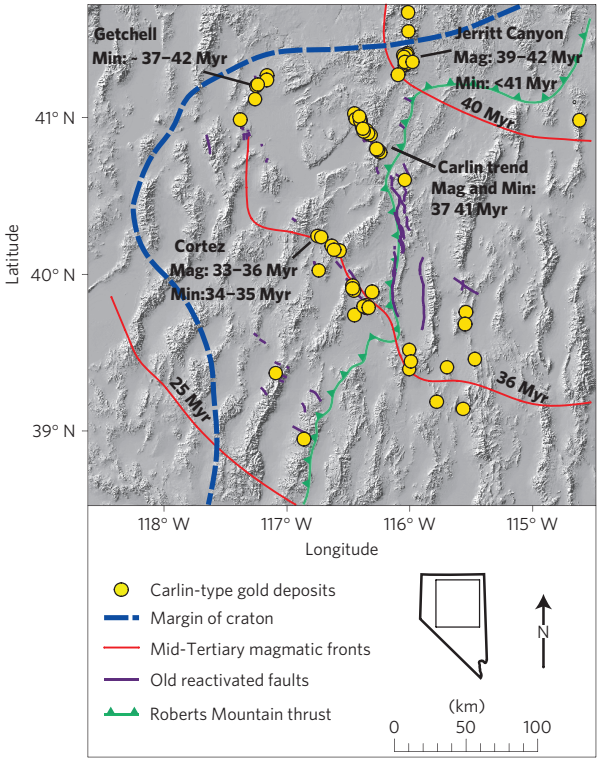

Figure 1 | Locations of CTGDs in northern Nevada. Locations of the four main clusters of CTGDs and their estimated age of mineralization (Min) and associated magmatism (Mag). Also shown are the margin of the underlying Precambrian craton (based on Sr isotopes), Mid-Tertiary magmatic fronts (limits of advance towards southern Nevada at indicated times), locations of old reactivated fault systems, and the easternmost extent of the Roberts Mountain thrust fault.

[1]Nevada Bureau of Mines and Geology, Mail Stop 178, University of Nevada Reno, Reno, Nevada, 89557-0178, USA, [2]University of Nevada, Las Vegas, Department of Geoscience, 4505 Maryland Parkway, PO Box 454010, Las Vegas, Nevada, 89514-4010, USA. *e-mail: munteanj@unr.edu.

Table 1 | Characteristics of CTGDs in Nevada.

1	Formed from 42 to 34 Myr BP, corresponding to a change from compression to extension and renewed magmatism in northern Nevada.
2	Occur in clusters along old, reactivated basement rift structures, preferentially hosted by carbonate-bearing rocks within or adjacent to structures in the lower plate of a regional thrust.
3	Similar hydrothermal alteration and ore paragenesis: dissolution and silicification of carbonate, sulphidation of Fe in the rock, formation of Au-bearing arsenian pyrite, and late open-space deposition of orpiment, realgar and stibnite. Ore signature is Au–Tl–As–Hg–Sb–(Te), with low Ag and base metals.
4	Non-boiling ore fluids ranged from ~180 to 240 °C and were of low salinity (mostly ≤6 wt% NaCl eq.) and CO_2-bearing (<4 mol %); illite and local kaolinite indicate acidic fluids.
5	Formation depth <3 km. Lack of mineral or elemental zoning at the scale of <5–10 km laterally and <2 km vertically suggests minor temperature gradients. No known coeval porphyry copper, skarn or distal Ag–Pb–Zn mineralization in the clusters of CTGDs.

magmatism in time and space across Nevada[1–4] (Fig. 1). Further support for a magmatic connection is provided by H and O isotope data collected from fluid inclusion waters and ore-stage quartz from the Getchell deposit[5] and from ore-stage kaolinite from some CTGDs (refs 1,2), which are consistent with mixtures of magmatic fluids and meteoric waters. Most other H and O isotope data suggest meteoric water as the source; however, we interpret these data as being consistent with titration of Au-bearing magmatic fluid into meteoric water (see Supplementary Data S1). Sulphur isotope data on ore-stage pyrite range from −4‰ to +13‰ δ^{34}S and are consistent with either a sedimentary or magmatic source[1] (see Supplementary Note S1). New laser ablation inductively coupled plasma mass spectrometry (LA-ICP-MS) analyses and electron probe microanalyses (see Supplementary Data S2) demonstrate that ore-stage pyrite contains Au along with As, Hg, Tl, Te, Cu and Sb, an elemental suite that is consistent with transport by magmatic aqueous vapour[6–9] (see Supplementary Note S2).

Development of optimal geologic setting

An essential first step in the origin of CTGDs was the formation of basement-penetrating rift structures that controlled development of favourable upper crustal structures and stratigraphy. Primarily northwest- and north-striking faults that formed during Mesoproterozoic construction of Rodinia and Neoproterozoic rifting of western North America[10,11] were critical in controlling subsequent patterns of sedimentation, deformation, magmatism and hydrothermal fluid flow[12,13]. Following active rifting, a predominantly carbonaceous, carbonate shelf-slope sequence formed along the margin. Reactivation of the underlying basement faults formed second-order basins with variable sedimentary facies, including carbonate debris flow breccias that are important hosts to CTGDs (refs 1,12,13). The Late Devonian to Early Mississippian Antler orogeny, the first in a series of compressional events, thrust deepwater siliciclastic and basaltic rocks eastward over the carbonate shelf-slope, forming the Roberts Mountain thrust fault. The compressional events reactivated underlying basement rift structures, forming fault propagation folds and other features consistent with structural inversion[13]. An optimal setting for the formation of CTGDs was established: structural culminations of highly fractured, reactive carbonate rocks were located above high-angle fault zones linked to underlying basement rift structures and capped by less reactive siliciclastic rocks (Fig. 2).

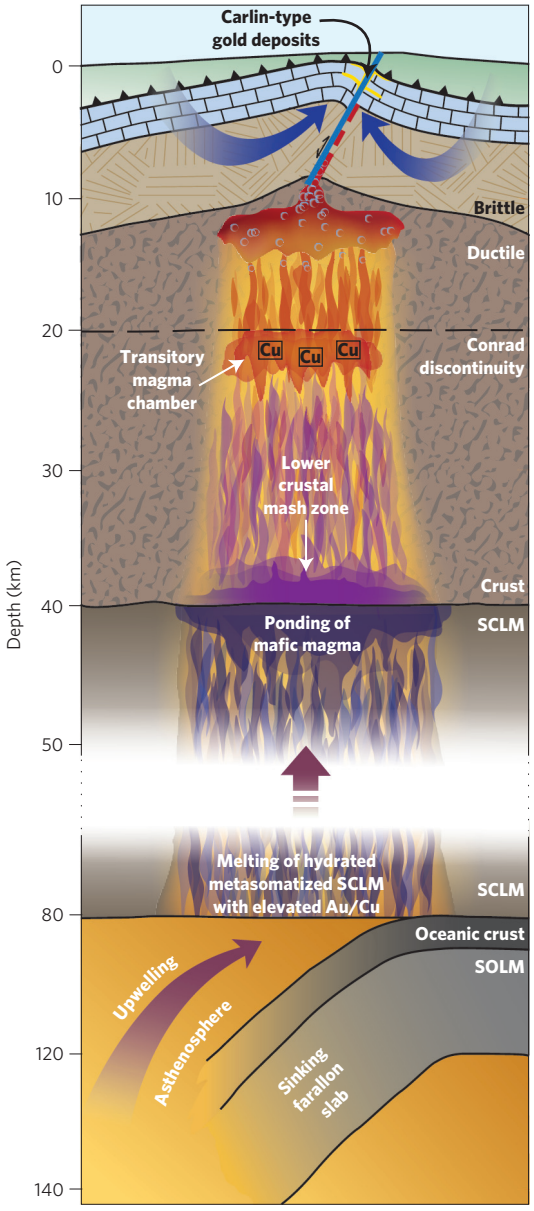

Figure 2 | Schematic cross-section from mantle to the surface (looking east). The points of the model discussed in the text are illustrated. SOLM signifies sub-oceanic lithospheric mantle.

Development of high Au/Cu magmas

A long-lived east-dipping subduction zone was established along western North America by the Middle Triassic period. Back-arc magmatism in Nevada began in the Middle to Late Jurassic period and ended by 65 Myr BP owing to flattening of the subducting Farallon slab[14]. During ~175 Myr of arc magmatism and slab dehydration, the mantle wedge beneath the Great Basin was continually hydrated[15] and metasomatized with metals including As, Sb, Tl, Pb, Cu (refs 16–18) and possibly Au (see Supplementary Note S3). Early moderately oxidized magmas may have fractionated a Au-rich sulphide residue during evolution of the subcontinental lithospheric mantle[19] (SCLM; see Supplementary Note S4). During the ~20 Myr of shallow subduction, from ~65 to 45 Myr BP, the base of the SCLM was further hydrated and metasomatized by slab-derived fluids[20].

Rollback or delamination of the shallow-dipping slab renewed magmatism at ~45 Myr BP (ref. 21), which swept southwestward at a high angle to the continental margin (Fig. 1). The base of

the fertile, hydrated, metasomatized SCLM with elevated Au/Cu (ref. 19) was exposed to upwelling asthenosphere, resulting in the formation of voluminous, CO_2-, Cl-, S- and Au-bearing, hydrous, high-alumina basaltic magmas, at an oxygen fugacity f_{O2} of ~FMQ + 1 (ref. 22; Fig. 2), where FMQ represents the fayalite–magnetite–quartz buffer. The basaltic magmas underplated and partially melted the overlying continental crust, forming hydrous, S- and Au-bearing, high-K, calc-alkaline magmas of intermediate composition[23] (Fig. 2). The magmas ascended and may have formed transitory magma chambers at the Conrad discontinuity (~20 km depth)[24], where we propose fractionation of monosulphide solid solution would have preferentially incorporated Cu over Au and further increased the Au/Cu ratio of the ascending melt (Fig. 2). Monosulphide solid solution (mss) is the only sulphide phase to crystallize owing to the low Cu concentration in the melt, which precluded formation of a Cu–Fe–S phase. New experimental data at an f_{O2} of ~FMQ + 1, $D_{Cu}^{mss/melt}$ ~ 3,600 and $D_{Au}^{mss/melt}$ ~ 490 (see Supplementary Data S3), confirm that monosulphide solid solution preferentially sequesters Cu relative to Au (see Supplementary Note S5).

Generation of ore fluid

As the magmas continued their ascent, they would have reached volatile saturation and released a single-phase (supercritical) CO_2-, H_2S- (at a high H_2S/SO_2 ratio; see Supplementary Note S6) and Au-bearing aqueous fluid with high Au/Cu (Fig. 2). A felsic magma containing 6 wt% H_2O and 1,000 ppm CO_2 would have released an aqueous phase at 400 MPa (~15–16 km, lithostatic pressure; see Supplementary Note S7). The salinity of this primitive ore fluid was probably between ~2 and 12 wt% NaCl eq., on the basis of analyses of fluid and melt inclusions from the deep parts of porphyry Cu deposits and Cl/OH ratios in amphiboles[16,25]. Experimental data demonstrate that Au and other metals strongly partition from the silicate melt to the volatile phase. For example, analyses of synthetic fluid inclusions trapped in felsic melt–volatile phase assemblages yield vapour/melt partition coefficients for Au ($D_{Au}^{vapour/melt}$) at 800 °C that range from 12 at 120 MPa with a 2 wt% NaCl eq. vapour, to 56 at 140 MPa with a 9 wt% NaCl eq. vapour[7,9]. Experimentally determined vapour/melt partition coefficients for Cu ($D_{Cu}^{aqueousfluid/melt}$), at similar conditions, are about 300 (ref. 8; see Supplementary Note S8).

Age–composition relationships of dykes and aeromagnetic data along the Carlin trend have identified six distinct Eocene igneous suites that are underlain by individual plutons emplaced at estimated depths of 3–10 km (ref. 3). The plutons comprise a large composite batholith (~10 × 40 km) that was assembled over 4 Myr. The ~36-Myr-old Harrison Pass pluton in the Ruby Mountains, located east of the Carlin trend, further supports the existence of deep Eocene batholithic intrusions. Hornblende geobarometry on this 14-km-diameter, composite granitic pluton suggests magma may have accumulated at a depth of ~20 km, before the pluton was emplaced at ~12 km, where a rheologic and density contrast between plutonic and metamorphic rocks and overlying sedimentary rocks was present[26]. Additional evidence for large Eocene magma bodies includes the 39.7-Myr-old Tuscarora caldera (16 km diameter), and the 33.9-Myr-old Caetano caldera that formed by eruption from a magma chamber that measured 20 km by 15 km at a depth of ~8–10 km (ref. 4). Both calderas formed within a million years of nearby CTGDs in the Carlin trend and Cortez district, respectively. From these data, we conclude that large volumes of Eocene magma stalled at depths of about 10 km near the brittle–ductile transition, forming batholithic-sized felsic intrusions owing to crystallization promoted by devolatilization, and density contrasts with less dense supracrustal rocks.

We conclude that single-phase, H_2S-rich aqueous fluids with high Au/Cu were tapped from reservoirs in the roof zones of plutons

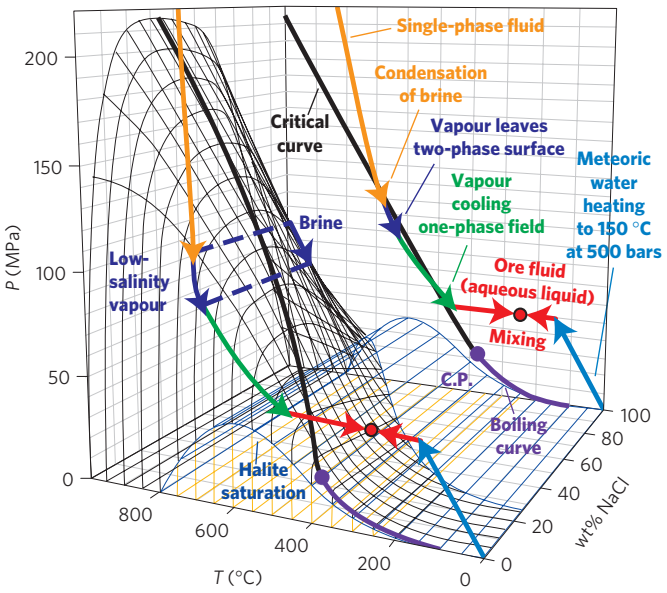

Figure 3 | Phase diagram of the NaCl–H_2O system. The two-phase liquid + vapour surface gridded by isopleths and isotherms is emphasized[30,32]. The critical curve (heavy black line at crest of two-phase surface) swings across from high salinities at high pressure and temperature (*P*, *T*) to lower salinities at lower *P* and *T*. The diagram shows fluid paths and important phase changes discussed in the text. The backface shows the projection of the critical curve and fluid paths onto the *P*–*T* plane. C.P. signifies the critical point of water.

during extensional reactivation of the high-angle faults linked to underlying basement rift structures (Fig. 2). Low-magnitude extension by pervasive rotational faulting locally occurred in northern Nevada between 36 and 40 Myr BP (refs 1,27). Periodic release of fluid and magma during faulting is supported by leucocratic cupola zones and porphyry roof dykes in the Harrison Pass pluton[26] and the numerous syn-ore dykes in the Carlin trend[2,3] and at Cortez[4]. We emphasize that tapping of fluids from magma bodies at ~10 km is significantly deeper than fluid release from magmas associated with typical porphyry Cu–(Au) and associated skarn deposits, which commonly form at depths of < ~ 4 km (ref. 6). Shallow release of high-temperature fluids from magma bodies associated with porphyry and skarn deposits results in large temperature gradients and strong zoning patterns in metals, ore mineralogy and hydrothermal alteration. Such zoning patterns are absent in CTGDs (Table 1).

The primitive ore fluid is interpreted to have separated into immiscible brine and vapour as it ascended along a high-angle fault zone away from its source magma (Figs 2 and 3). For example, a 900 °C aqueous fluid with a salinity of 10 wt% NaCl eq. that cooled adiabatically during ascent from a pressure of 300 MPa (orange arrows in Fig. 3) would have condensed a small amount of brine with a salinity of 38 wt% NaCl eq. at 690 °C and 115 MPa. If vapour and brine continued to ascend and cool together, for example to 95 MPa and 653 °C, 84% of the bulk fluid would be vapour with a salinity of 3.85 wt% NaCl eq. and a density of 0.34 g cm^{-3}; the remaining 16% would be brine with a salinity of 42.9 wt% NaCl eq. and a density of 0.85 g cm^{-3} (blue arrows in Fig. 3; ref. 28; see Supplementary Note S9).

Upon fluid separation, metals would have partitioned between the vapour and brine. LA-ICP-MS analyses of both natural and synthetic fluid inclusions demonstrate significant quantities of Au, Cu, As, Sb and S can be transported by vapour, whereas Fe, Ag, Pb, Zn and Mn partition strongly into brine[6,29] (see Supplementary Note S10). These empirical data demonstrate,

first, significant mass transport of Au by vapour and of Fe by brine, and second, separation of brine was critical to preferentially remove Fe and develop a high S/Fe ratio in the vapour that transported Au. Had abundant Fe remained in the S- and Au-bearing low-salinity vapour, pyrite would have precipitated during fluid ascent, destabilizing aqueous Au–sulphide complexes, and Au would have precipitated continuously along the fluid conduit, greatly reducing the amount of Au transported to the level of CTGDs (ref. 30). During fluid ascent and cooling, increasing differences in density would have promoted departure of the vapour from the solvus, leaving the brine at depth[6] (green arrow in Fig. 3). We propose this rising hot Au-bearing vapour plume with a salinity of ~3–5 wt% NaCl eq. entrained meteoric water as it rose through the upper crust[31] (light blue arrows in Fig. 3). The mixing with meteoric water (red arrows in Fig. 3) would have increased the cooling rate of the ascending plume, potentially causing the plume to pass over the critical curve (black line in Fig. 3) by near-isobaric cooling and evolve into a liquid without further phase separation[30] (red arrows pointing right in Fig. 3). Enthalpy–salinity relationships and calculations in conjunction with O and H isotope data from some CTGDs (ref. 1) indicate that incorporation of a reasonable quantity of meteoric water by the vapour readily produces an ore fluid of ~250 °C and ~2–3 wt% NaCl eq., consistent with upper temperatures determined for fluid inclusions in CTGDs (ref. 1; see Supplementary Note S11).

Along much of the fluid pathway, fluid acidity was probably buffered by the rock[32]; however, the fluid would have evolved to become acidic at $< \sim 350$ °C owing to dissociation of carbonic acid[33] ($H_2CO_3 \Rightarrow H^+ + HCO_3^-$), probably the most important acid in the ore fluid on the basis of quadrupole mass spectrometer gas analyses of fluid inclusions in CTGDs (ref. 5; see Supplementary Note S12). The contrast between reactive carbonate rocks and overlying thrust plates of relatively impermeable, less reactive siliciclastic rocks, under hydrostatic pressure near the surface, is interpreted to have caused the now acidic ore fluid to leave high-angle fault zones and infiltrate the highly fractured carbonate country rocks at depths of <3 km. Dissolution of carbonate increased permeability, facilitating fluid flow into the country rocks and leading to further fluid–rock reaction.

Efficient gold deposition

Key to the formation of CTGDs was an effective, efficient depositional mechanism. Au occurs in arsenian and trace-element-rich pyrite in replaced wall rocks; open-space deposition of Au-bearing pyrite is rare[1], indicating that fluid–rock reaction was the main cause of Au deposition. Au-bearing pyrite occurs as rims on pre-ore pyrite, or as micrometre-scale spheroidal 'fuzzy' grains (Fig. 4; see Supplementary Data S2). X-ray adsorption near-edge structure, extended X-ray adsorption fine structure and secondary-ion mass spectroscopy analyses demonstrate some Au in pyrite is present as submicrometre inclusions of native Au^0 but dominantly occurs as structurally bound Au^{1+}, which allows transport and deposition of Au by fluids that were not necessarily saturated with respect to native Au^0 (refs 34,35). Deposition of Au was caused by reaction of reduced Au-sulphide species in the ore fluid with Fe^{2+} in the host rock to form pyrite[36]. Loss of sulphide from the ore fluid destabilized Au–sulphide complexes and resulted in incorporation of Au and other trace metals in pyrite including primarily As, Hg, Cu, Sb, Tl and Te. Recently recognized and quantified variations in pyrite rim chemistry at the Turquoise Ridge deposit (see Supplementary Data S2) are interpreted to reflect variations in metal concentrations in the ore fluid, and zoned rims indicate that pulses of chemically distinct ore fluids delivered Au and trace metals to the deposit[37] (Fig. 4). The incompatible element-rich

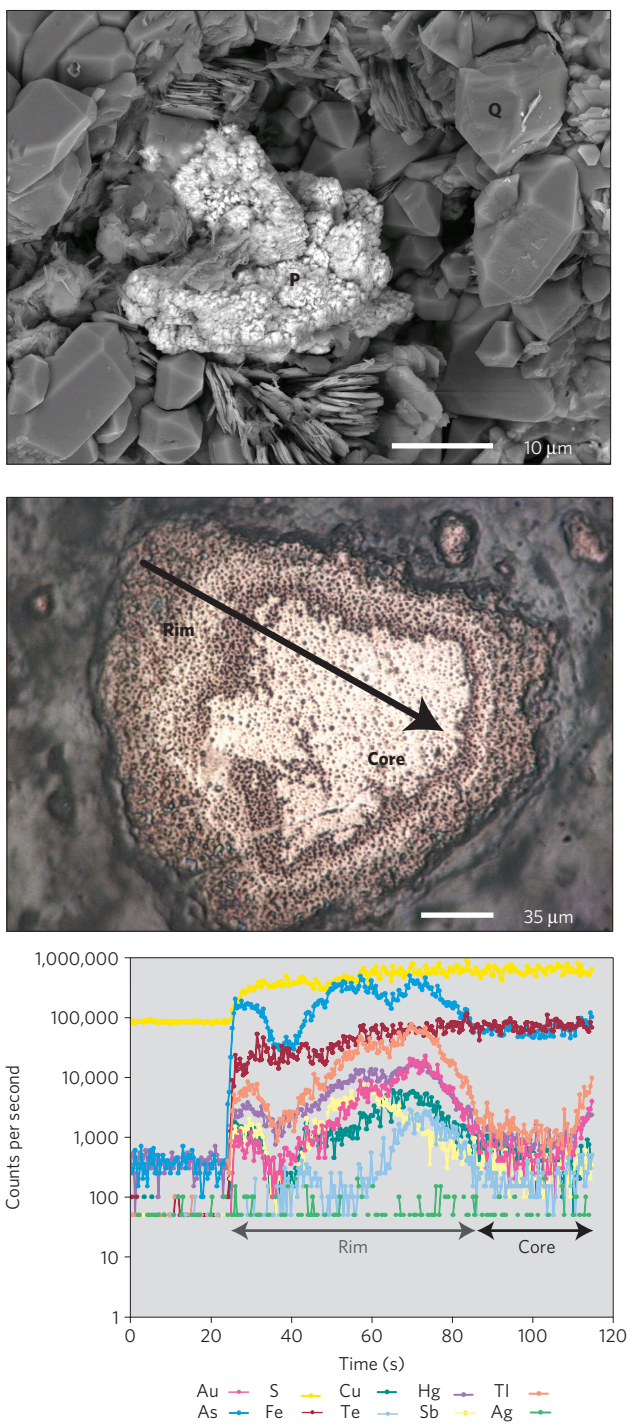

Figure 4 | Images and analyses of ore-stage pyrite. a, Scanning electron micrograph of ore from the Turquoise Ridge CTGD, consisting of quartz (Q), kaolinite (K) and pyrite (P). **b**, Back-scattered electron image of pyrite from Turquoise Ridge showing pre-ore core and ore-stage rim and location of LA-ICP-MS transect. **c**, Results of LA-ICP-MS transect showing a marked increase in trace elements from core to rim. Counts are directly related to concentrations of the analysed isotopes and reveal an inner rim with highest Au, Tl, Hg, Cu and Te, and a narrow outer rim with high Au, Tl, Hg, Cu and Sb.

pyrite composition reflects earlier metal partitioning between melt and the primitive ore fluid and between vapour and brine, and is consistent with vapour transport of metals. Sulphidation as the principle precipitation mechanism is supported on the scale of

individual deposits by lithogeochemical studies that indicate S was added to rock containing varying amounts of Fe (ref. 38). Ore formation was probably facilitated by extremely efficient scavenging of Au through adsorption of Au^{1+} onto negatively charged pyrite surfaces, from acidic fluids that were undersaturated with respect to native Au^0 (ref. 39; see Supplementary Note S13). Late-ore-stage mineralization, characterized by open-space deposition of drusy quartz, orpiment, realgar and stibnite with little to no associated Au, is best explained by cooling[36], which was related to the collapse of the hydrothermal system and incursion of near-surface meteoric waters.

CTGDs reflect a major thermal and mass transfer event in the Great Basin during which CTGDs formed along with other types of ore deposits including the giant Bingham Canyon porphyry Cu–Au–Mo and Mount Hope porphyry Mo deposits. The large number and variety of ore deposits that formed during this event are an indication of multiple evolutionary paths for magma and their evolved ore fluids. Such major thermal events and magma and hydrothermal fluid pathways, including the one outlined here for CTGDs, are not necessarily unique to the Great Basin. The clusters and varieties of large Neoarchean gold deposits in the Superior craton of eastern Canada and the Yilgarn craton of Western Australia also formed during major crustal-scale thermal events from multiple fluid pathways[40].

As the magmatic–hydrothermal processes in CTGDs are not geologically unusual, the apparent restriction of CTGDs to Nevada represents a convergence of these processes with an ideal geological setting that is specific to Nevada—that is, a deformed, carbonate-bearing, continental margin that was underlain by SCLM, which itself was modified by ~175 Myr of subduction-induced fertilization. It is this convergence that created an ideal system for the formation of CTGDs. The critical trigger was the rollback of the shallow Farallon slab that caused the asthenosphere to impinge on strongly hydrated and trace-metal-enriched SCLM, resulting in profuse magmatism. Au-bearing aqueous fluids were generated, transported, and focused into reactive carbonate wall rocks. Ore fluids dissolved and sulphidized Fe-bearing carbonate rocks, and Au adsorbed onto newly precipitated pyrite in an extremely effective depositional mechanism.

Received 17 February 2010; accepted 14 December 2010; published online 23 January 2011

References

1. Cline, J. S., Hofstra, A. H., Muntean, J. L., Tosdal, R. M. & Hickey, K. A. in *Economic Geology 100th Anniversary Volume* (eds Hedenquist, J. W., Thompson, J. F. H., Goldfarb, R. J. & Richards, J. P.) 451–484 (Society of Economic Geologists, 2005).
2. Heitt, D. G., Dunbar, W. W., Thompson, T. B. & Jackson, R. G. Geology and geochemistry of the Deep Star gold deposit, Carlin trend, Nevada. *Econ. Geol.* **98,** 1107–1136 (2003).
3. Ressel, M. W. & Henry, C. D. Igneous geology of the Carlin trend, Nevada: Development of the Eocene plutonic complex and significance for Carlin-type gold deposits. *Econ. Geol.* **101,** 347–383 (2006).
4. John, D. A., Henry, C. D. & Colgan, J. P. Magmatic and tectonic evolution of the Caetano caldera, north-central Nevada: A tilted, mid-Tertiary eruptive center and source of the Caetano tuff. *Geosphere* **4,** 75–106 (2008).
5. Cline, J. S. & Hofstra, A. H. Ore fluid evolution at the Getchell Carlin-type gold deposit, Nevada, USA. *Eur. J. Mineral.* **12,** 195–212 (2000).
6. Williams-Jones, A. E. & Heinrich, C. A. Vapor transport of metals and the formation of magmatic-hydrothermal ore deposits. *Econ. Geol.* **100,** 1287–1312 (2005).
7. Simon, A. C. *et al.* Gold partitioning in melt-vapor-brine systems. *Geochim. Cosmochim. Acta* **69,** 3321–3335 (2005).
8. Simon, A. C., Pettke, T., Candela, P. A., Piccoli, P. M. & Heinrich, C. A. Copper partitioning in a melt-vapor-brine-magnetite–pyrrhotite assemblage. *Geochim. Cosmochim. Acta* **70,** 5583–5600 (2006).
9. Simon, A. C., Pettke, T., Candela, P. A., Piccoli, P. M. & Heinrich, C. A. The partitioning behavior of As and Au in S-free and S-bearing magmatic assemblages. *Geochim. Cosmochim. Acta* **71,** 1764–1782 (2007).
10. Tosdal, R. M., Wooden, J. L. & Kistler, R. W. in *Geology and Ore Deposits 2000: The Great Basin and Beyond* (eds Cluer, J. K., Price, J. G., Struhsacker, E. M., Hardyman, R. F. & Morris, C. L.) 451–466 (Geological Society of Nevada, 2000).
11. Marshak, S., Karlstrom, K. & Timmons, J. M. Inversion of Proterozoic extensional faults: An explanation for the pattern of Laramide and Ancestral Rockies intracratonic deformation, United States. *Geology* **28,** 735–738 (2000).
12. Emsbo, P., Groves, D. I., Hofstra, A. H. & Bierlein, F. P. The giant Carlin gold province: A protracted interplay of orogenic, basinal, and hydrothermal processes above a lithospheric boundary. *Min. Dep.* **41,** 517–525 (2006).
13. Muntean, J. L., Coward, M. P. & Tarnocai, C. A. in *Deformation of the Continental Crust: The Legacy of Mike Coward* 272 (eds Reis, A. C., Butler, R. W. H. & Graham, R. H.) 571–587 (Spec. Publ. Geol. Soc. Lond., 2007).
14. Coney, P. J. & Reynolds, S. J. Cordilleran Benioff zones. *Nature* **270,** 403–406 (1977).
15. Iwamori, H. Transportation of H_2O and melting in subduction zones. *Earth Planet. Sci. Lett.* **160,** 65–80 (1998).
16. Candela, P. A. & Piccoli, P. M. in *Economic Geology 100th Anniversary Volume* (eds Hedenquist, J. W., Thompson, J. F. H., Goldfarb, R. J. & Richards, J. P.) 25–37 (Society of Economic Geologists, 2005).
17. Noll, P. D., Newsom, H. W., Leeman, W. P. & Ryan, J. G. The role of hydrothermal fluids in the production of subduction zone magmas: Evidence from siderophile and chalcophile trace elements and boron. *Geochim. Cosmochim. Acta* **60,** 587–611 (1996).
18. Hattori, K. H. & Guillot, S. Volcanic fronts form as a consequence of serpentine dehydration in the forearc mantle wedge. *Geology* **31,** 525–528 (2003).
19. Richards, J. P. Postsubduction porphyry Cu–Au and epithermal Au deposits: Products of remelting of subduction-modified lithosphere. *Geology* **37,** 247–250 (2009).
20. Humphreys, E. *et al.* How Laramide-age hydration of North American lithosphere by the Farallon slab controlled subsequent activity in the western United States. *Int. Geol. Rev.* **45,** 575–595 (2003).
21. Humphreys, E. D. Post-Laramide removal of the Farallon Slab, western United States. *Geology* **23,** 987–990 (1995).
22. Kelley, K. A. & Cottrell, E. Water and the oxidation state of subduction zone magmas. *Science* **325,** 605–607 (2009).
23. Gans, P. B., Mahood, G. A. & Schermer, E. Synextensional magmatism in the Basin and Range province: A case study from the eastern Great Basin. (Special Paper Vol. 233, Geological Society of America 1989).
24. Annen, C., Blundy, J. D. & Sparks, R. S. J. The genesis of intermediate and silicic magmas in deep crustal hot zones. *J. Petrol.* **47,** 505–539 (2006).
25. Redmond, P. B., Einaudi, M. T., Inan, E. E., Landtwing, M. R. & Heinrich, C. A. Copper deposition from fluid cooling in intrusion-centered system: New insights from the Bingham porphyry ore deposit, Utah. *Geology* **32,** 217–220 (2004).
26. Barnes, C. G., Burton, B. R., Burling, T. C., Wright, J. E. & Karlsson, H. R. Petrology and geochemistry of the late Eocene Harrison Pass pluton, Ruby Mountains core complex, northeastern Nevada. *J. Petrol.* **42,** 901–929 (2001).
27. Henry, C. D. Ash-flow tuffs and paleovalleys in northeastern Nevada: Implications for Eocene paleogeography and extension in the Sevier hinterland, northern Great Basin. *Geosphere* **4,** 1–35 (2008).
28. Driesner, T. & Heinrich, C. A. The system H_2O–NaCl. Part I: Correlation formulae for phase relations in temperature–pressure-composition space from 0 to 1000 °C, 0 to 5000 bar, and 0 to 1 X_{NaCl}. *Geochim. Cosmochim. Acta* **71,** 4880–4901 (2007).
29. Seo, J. H., Guillong, M. & Heinrich, C. A. The role of sulfur in the formation of magmatic-hydrothermal copper–gold deposits. *Earth Planet. Sci. Lett.* **282,** 323–328 (2009).
30. Heinrich, C. A., Driesner, T., Stefánsson, A. & Seward, T. M. Magmatic vapor contraction and the transport of gold from the porphyry environment to epithermal ore deposits. *Geology* **32,** 761–764 (2004).
31. Henley, R. W. & McNabb, A. Magmatic vapor plumes and ground-water interaction in porphyry copper emplacement. *Econ. Geol.* **73,** 1–20 (1978).
32. Giggenbach, W. F. Magma degassing and mineral deposition in hydrothermal systems along convergent plate boundaries. *Econ. Geol.* **87,** 1927–1944 (1992).
33. Heinrich, C. A. The chemistry of hydrothermal tin-(-tungsten) ore deposition. *Econ. Geol.* **85,** 457–481 (1990).
34. Simon, G., Kesler, S. E. & Chryssoulis, S. Geochemistry and textures of gold-bearing arsenian pyrite, Twin Creeks, Nevada: Implications for deposition of gold in Carlin-type deposits. *Econ. Geol.* **94,** 405–422 (1999).
35. Reich, M. *et al.* Solubility of gold in arsenian pyrite. *Geochim. Cosmochim. Acta* **69,** 2781–2796 (2005).
36. Hofstra, A. H. *et al.* Genesis of sediment-hosted disseminated gold deposits by fluid mixing and sulfidization: Chemical-reaction-path modeling of ore-depositional processes documented in the Jerritt Canyon district, Nevada. *Geology* **19,** 36–40 (1991).
37. Barker, S. L. *et al.* Uncloaking invisible gold: Use of nanoSIMS to evaluate gold, trace elements and sulfur isotopes in pyrite from Carlin-type gold deposits. *Econ. Geol.* **104,** 897–904 (2009).

38. Stenger, D. P., Kesler, S. E., Peltonen, D. R. & Tapper, C. J. Deposition of gold in Carlin-type deposits: The role of sulfidation and decarbonation at Twin Creeks, Nevada. *Econ. Geol.* **93,** 210–215 (1998).
39. Widler, A. M. & Seward, T. M. The adsorption of gold(I) hydrosulfide complexes by iron sulphide surfaces. *Geochim. Cosmochim. Acta* **66,** 383–402 (2002).
40. Robert, F., Poulsen, K. H., Cassidy, K. F. & Hodgson, C. J. in *Economic Geology 100th Anniversary Volume* (eds Hedenquist, J. W., Thompson, J. F. H., Goldfarb, R. J. & Richards, J. P.) 1001–1033 (Society of Economic Geologists, 2005).

Acknowledgements

This work was supported by the National Science Foundation (EAR awards 0635657 to J.L.M., 0635658 to J.S.C. and 0609550 to A.C.S.), the US Geological Survey's Mineral Resources External Research Program, Placer Dome Exploration and Barrick Gold Corporation.

Author contributions

J.L.M., J.S.C., A.C.S. and A.A.L. conceived the model for the CTGDs. J.L.M. took the lead in preparation of the manuscript and figures and contributed Supplementary Data S1. J.S.C. and A.A.L. contributed Supplementary Data S2 and A.C.S. contributed Supplementary Data S3.

Additional information

The authors declare no competing financial interests. Supplementary information accompanies this paper on www.nature.com/naturegeoscience. Reprints and permissions information is available online at http://npg.nature.com/reprintsandpermissions. Correspondence and requests for materials should be addressed to J.L.M.